Picosecond phonon dynamics and self-energy effects in highly photoexcited germanium

M. L. Ledgerwood and H. M. van Driel
Department of Physics, University of Toronto, 60 St. George Street, Toronto, Canada M5S 1A7
(Received 25 March 1996)

Self-energies and population kinetics of optical phonons in strongly photo-excited intrinsic and p-type doped germanium have been studied using picosecond Raman scattering measurements at 295 K for induced carrier densities up to 2×10^{20} cm^{-3}. Time-integrated and time-resolved measurements indicate that the nonequilibrium phonon occupation number increases sublinearly and its temporal peak shifts as the photoexcited carrier density is increased above 10^{19} cm^{-3}. A theoretical model of coupled carrier and phonon dynamics indicates that this can be attributed to nonequilibrium phonon reabsorption by holes undergoing intra-heavy-hole valence-band transitions. The time-integrated measurements also reveal broadening and shifting of the Raman lines: for a photoexcited carrier density of 2×10^{20} cm^{-3}, the line broadening indicates that the phonon lifetime is reduced from its quiescent value of 4 ps to $\sim$ 0.5 ps and the phonon frequency is reduced by $\sim$8 cm^{-1}. We present a microscopic model to describe the phonon self-energy effects that are caused by carrier-phonon interactions. The model indicates that the phonon broadening is consistent with primarily intra-heavy-hole valence-band transitions, while the phonon frequency renormalization is consistent with primarily inter-heavy-hole$\leftrightarrow$light-hole valence-band transitions. [S0163-1829(96)00631-5]

I. INTRODUCTION

Incoherent Raman spectroscopy with either continuous wave (cw) or picosecond pulsed light sources is a useful probe of near-zone-center, longitudinal optical (LO) and transverse optical (TO) phonons in Group IV and III-V semiconductors. For example, the broadening and shifting of cw Raman lines with increasing lattice temperature gives a frequency-domain view of the influence of the anharmonic interaction on the phonon lifetime and frequency.[1–3] Shifted and asymmetrically broadened cw Raman spectra in heavily doped extrinsic semiconductors have revealed the contribution of carrier-phonon interactions to the phonon self-energy.[4–6] Time-resolved incoherent Raman spectroscopy provides an alternative method for probing LO and TO phonon dynamics and lifetimes in group-IV and -III-V semiconductors.[7–14] In the first such measurements, von der Linde *et al.*[7] used picosecond pulses to probe the temporal evolution of nonequilibrium phonon populations and determined the lifetime of LO phonons in GaAs at 77 K to be $\sim$ 4 ps. Since then, time-resolved Raman measurements have allowed direct determinations of the phonon lifetime dependence on lattice temperature in Ge and GaAs,[8,10,11] alloy composition in group-IV and -III-V alloys,[9,14] and isotopic composition in Ge.[13]

It has been suggested that under intense excitation, hot phonon reabsorption by a dense intrinsic plasma should reduce the cooling rate of photoexcited carriers[15–17] and inhibit the buildup of nonequilibrium phonons. This carrier-phonon phenomenon, commonly referred to as the *hot phonon effect*, has been cited to explain reduced carrier cooling rates in Ge (Ref. 15) and GaAs.[16,18] The presence of phonon reabsorption and a concomitant reduction in phonon lifetime in GaAs (Ref. 19) and III-V quantum wells[20] have been confirmed by time-integrated and time-resolved Raman measurements. Earlier, we presented preliminary results on picosecond Raman measurements of LO phonons in highly photoexcited Ge that suggested an influence of phonon reabsorption on phonon lifetime and an influence of many-body effects on phonon broadening.[21,22]

In this work, we report the use of picosecond time-resolved and time-integrated Raman spectroscopy to *simultaneously* perform time-domain studies of LO phonon dynamics and frequency-domain studies of LO phonon self-energy effects in the presence of a hot photoexcited plasma with carrier density $N\sim10^{20}$ cm^{-3} in intrinsic and p-type doped Ge at 295 K. The carrier densities are substantially higher than those of previous picosecond Raman studies of Ge,[10–13] all of which gave results consistent with scaling of the phonon population with excitation intensity, and a carrier-density-independent phonon decay rate. We report sublinear increases in the phonon occupation number and Raman linewidth and a sublinear decrease in the phonon frequency as the density of the optically injected plasma is increased. A theoretical model of coupled carrier and phonon kinetics in the high excitation regime suggests that the sublinear increase in phonon occupation number can be primarily attributed to an increase in nonequilibrium phonon absorption by carriers with increasing N.[22] We also present a theoretical model of phonon self-energy effects (phonon line broadening and frequency renormalization) in the presence of hot carriers, which indicates that the observed Raman line broadening and frequency shift are associated with intra- and inter-valence-band single-particle excitations.[23]

The rest of this paper is organized as follows. Section II contains a description of the experimental apparatus used in picosecond time-resolved and time-integrated Raman scattering measurements. Section III presents the phonon self-energy and coupled carrier-phonon dynamics models used to analyze the Raman spectroscopy data. In Sec. IV measurements of broadening and shifting of the Raman lines with increasing N are compared to simulations of the Raman linewidth and line shift based on the phonon self-energy model. Measured Raman intensities are used to determine the tem-

poral evolution of the phonon occupation number, and the N dependence of the time-integrated phonon occupation number; these measurements are compared to simulations based on the coupled carrier-phonon dynamics model. Key results and conclusions of this work are given in Sec. V.

II. EXPERIMENTAL DETAILS

Two types of Raman scattering experiments—time-integrated and time-resolved—were performed at 295 K to probe LO phonons in crystalline intrinsic and p type doped (with acceptor densities of $N_a=2\times10^{19}$ and 5×10^{19} cm^{-3}) Ge (001). Both experiments involved exciting and probing samples with 3–4 ps [full width at half maximum (FWHM)] light pulses; these are short enough and spectrally narrow enough to offer both good temporal resolution and reasonable spectral resolution. The experiments used a standard pump-probe configuration similar to that described elsewhere,[12] with the exception that the excitation dye laser was cavity dumped to provide more energetic light pulses (up to $\sim$ 30 nJ) than those used by previous workers.[11–13] The laser was configured to produce $\lambda = 585$ nm light pulses at a repetition rate of 9.5 MHz. For both types of experiments, the probe beam polarization was parallel to the (010) direction. First-order Raman-scattered light from the probe beam was collected in a backscattering geometry, analyzed with a triple spectrometer, and monitored on a charge coupled device array detector. The experimental configuration probes LO phonons with quiescent energy $E_{q_0}=37$ meV and wave number $q_0=1.2\times10^6$ cm^{-1}; symmetry dictates that the behavior of TO phonons is essentially identical.

In the first type of experiment, time-integrated Stokes and anti-Stokes Raman spectra were measured as a function of light pulse fluence using a single train of pulses to study the N dependence of the phonon occupation number, frequency, and linewidth. The pulses were focused to an $\sim$ 15-μm-diam spot, with fluences up to $\sim$ 4 $\mathrm{mJ/cm}^2$ per pulse and carrier densities up to $\sim2\times10^{20}\mathrm{cm}^3$. [Quoted fluences F are transverse spatial averages of the energy density per light pulse. All quoted photoexcited carrier densities N refer to the transverse spatial average and the temporal peak in the density of free carriers at the surface of the sample. N is calculated according to the light pulse fluence and duration using an absorption coefficient of 3×10^5 cm^{-1} and Othonos, van Driel, Young, and Kelly's (ODYK's) model.[12] These N values have a systematic uncertainty of $\pm$ 40%, due to the experimental uncertainty in fluence. The random error in N, associated with fluctuations in the pulse energy, is $\pm$ 10%.] The second type of experiment used orthogonally polarized pump and probe pulses to time resolve the Stokes and anti-Stokes scattering intensities. Spatial averaging effects were reduced by focusing the pump beam to a spot $\sim$ 30 μm in diameter, twice the diameter of the probe spot. Each pump pulse had $F\sim2$ $\mathrm{mJ/cm}^2$ in the probed area, 4$\times$ the fluence of each probe pulse.

The Raman line broadening and frequency shift with increasing N were quantified by measuring the anti-Stokes Raman line FWHM and line center at half maximum (LCHM) relative to empirically determined values of the $N\rightarrow0$, room-temperature anti-Stokes FWHM ($2\Gamma_0$) and LCHM. Line broadening is of interest, rather than the absolute linewidth since the linewidth includes the $N=0$ room-temperature phonon linewidth, the probe band width, the spectrometer response function, sample inhomogeneity, pure dephasing events, and inhomogeneous line broadening. The LCHM rather than the position of the line peak was used to quantify the line shift because the high-N Raman lines are asymmetric. (The random errors in the measured linewidths and line positions are $\pm\sim$ 0.5 cm^{-1}. The systematic uncertainties in the measured linewidth increases and line shifts, associated with the uncertainties in the $N\rightarrow0$ FWHM and LCHM, are $\pm$ 1 cm^{-1}.)

Measurements of the dependence of the time-integrated phonon occupation number on photoexcited carrier density $n(N)$ and of the time-resolved phonon occupation number $n(t)$ are based on measured Stokes–anti-Stokes intensity ratios. Because of the line broadening, integrated intensities of the Stokes and anti-Stokes Raman lines (I_S and I_{AS} respectively), rather than the Raman line heights, were used to measure Stokes–anti-Stokes intensity ratios. The use of I_S and I_{AS} to probe n can be complicated by the potential for (i) unequal collection and/or detection efficiencies of the Stokes and anti-Stokes light and (ii) changes in the Stokes and anti-Stokes cross sections with carrier density.[24,25] These complications are addressed by the factor Q in

$$n=\left(Q\frac{I_S}{I_{AS}}-1\right)^{-1}. \tag{1}$$

For a fixed excitation wavelength Q can be determined empirically using

$$Q=\frac{n^{\mathrm{eq}}+1}{n^{\mathrm{eq}}}\left(\frac{I_{AS}}{I_S}\right)_{F\rightarrow0}, \tag{2}$$

where n^{eq} is the room-temperature equilibrium phonon occupation number and $(I_{AS}/I_S)_{F\rightarrow0}$ is given by extrapolation of low excitation anti-Stokes–Stokes ratios to negligible excitation. The uncertainty in Q, associated with the uncertainty in $(I_{AS}/I_S)_{F\rightarrow0}$, is $\pm$ 15%. The corresponding systematic uncertainty in n increases with n, from $\pm$ 25% for $n\approx$ 0.5, to $\pm$ 50% for $n\approx$ 2. We assume that the low-excitation value of Q can be applied to high excitation measurements, which is roughly equivalent to assuming that the ratio σ_{AS}/σ_S is constant. The validity of this assumption must be carefully considered because of the proximity of the excitation wavelength to the E_1 and $E_1+\Delta_1$ resonance in the Raman scattering cross section of Ge and observations of a redshift and reduction in strength of this resonance in the presence of hole or electron densities exceeding 10^{19} cm^{-3}.[24,25] These observations suggest that, for an excitation frequency below the Raman resonance peak, both σ_S and σ_{AS} may decrease with increasing N in intrinsic Ge. However, the reduction in the ratio σ_{AS}/σ_S, inferred from the data for p-type doped Ge,[25] is small ($<$ 5% for $N_a=4\times10^{19}$ cm^{-3}). Thus it is reasonable to assume that Q is constant for the range of photoexcited carrier densities produced in the experiments. Note that steady-state and transient lattice temperature increases are small enough that lattice heating-induced changes in the Raman resonance profile[2] can be neglected. With the assumptions that both Q and σ_{AS}/σ_S are constant, the mea-

sured Stokes and anti-Stokes intensities can also be used to measure relative changes in the Raman scattering cross section

$$\sigma_{AS} \propto \sigma_S \propto I_S - \frac{I_{AS}}{Q}. \tag{3}$$

Interpretation of the phonon occupation number, Raman line broadening, and shifting data requires some care since the samples are excited and probed with spatially and temporally Gaussian, finite bandwidth pulses. The simulations presented in Sec. IV include convolution effects associated with the excitation and/or probing conditions; neglect of these effects causes the line broadening to be underestimated (by $\sim$ 10%) and both the line shift and phonon occupation number to be overestimated (by 30% and 20%, respectively), for $N = 2 \times 10^{20}$ cm^{-3}.

III. THEORETICAL MODELS

In group-IV semiconductors, carriers and phonons interact through the deformation potential. This interaction causes the contribution of photoexcited carriers to the phonon self-energy through single-particle excitations (SPE's) and the generation or absorption of nonequilibrium phonons through carrier cooling or reexcitation. According to ODYK's low-excitation model,[12] hole cooling and, to a lesser extent, electron cooling produce a nearly monoenergetic distribution of LO and/or TO phonons, with an *effective* temperature that exceeds the lattice temperature. On a picosecond time scale, the carriers cool to the effective temperature of the nonequilibrium optical phonons; subsequently their rate of cooling is determined by the rate of energy transfer from the LO and/or TO phonons to the lattice. Once the carrier, LO and/or TO phonon, and lattice systems attain thermal equilibrium, the excited volume returns to equilibrium with the rest of the sample on a slower ($\sim$ nsec) time scale through carrier and heat diffusion. With the exception of negligible residual lattice heating, the combined carrier and lattice system completely recovers by the time the next light pulse arrives.

The *high* excitation regime differs from that described above in the following ways. (i) With a high density of hot photoexcited holes, SPE's may broaden the phonon and renormalize the phonon energy. These effects would be similar to Raman line broadening and shifting observed in heavily p-type doped Ge (Ref. 5) with *cold* hole densities of the order of 10^{20} cm^{-3}. (ii) The hot phonon effect[15,17] may be important. (iii) The residual lattice heating produced by each light pulse will be sufficient to raise the steady-state lattice temperature and reduce the phonon lifetime and energy through anharmonic interactions.[1–3]

A. Phonon self-energy in germanium

The $T = 0$ contribution of intra-heavy-hole SPE's to the phonon self-energy in Ge has been calculated by Olego and Cardona.[5] Here we extend Olego and Cardona's model to calculate the contribution of hot carrier-phonon interactions to the phonon self-energy. Our model also includes both intra-heavy-hole and inter-heavy-hole$\leftrightarrow$light-hole SPE's; this is essential to predict accurately the real part of the phonon self-energy (i.e., the phonon frequency shift).

The SPE contribution to the phonon self-energy, $\Sigma = -\Delta E + i\Delta\Gamma$, is calculated by considering single-phonon–single-carrier processes in which a phonon is created or annihilated simultaneously with the annihilation or creation of a free carrier.[5,26] Here ΔE is the phonon energy shift and $2\Delta\Gamma$ is the phonon linewidth change (in energy units). Calculating Σ is equivalent to calculating the (intraband and interband) dielectric susceptibility and can therefore take advantage of the relation between the real and imaginary parts of the phonon self-energy through the Kramers-Kronig relation. We begin with Fermi's golden rule

$$\Delta\Gamma(E_q, q) = \frac{D_c^2 \hbar}{4\tilde{\rho} c E_q} \rho(E_q, q), \tag{4}$$

where ρ is the density of SPE's involving a phonon with energy E_q and wave vector q, D_c ($c = H$ for holes, $c = E$ for electrons) is the deformation potential constant, $\tilde{\rho}$ is the mass density, and c is the speed of light. The real part of the SPE self-energy contribution is then given by the Hilbert (or Kramers-Kronig) transform of the imaginary part

$$\Delta E(E_q, q) = \frac{D_c^2 \hbar}{4\pi\tilde{\rho} c E_q} \mathcal{P} \int_0^\infty \rho(E, q) \left\{ \frac{1}{E_q - E} - \frac{1}{E_q + E} \right\} dE. \tag{5}$$

In general, SPE's involving both electrons and holes can contribute to the phonon self-energy. However, for optical phonons in Ge, SPE's within the conduction bands can be neglected since (i) the electron intravalley deformation potential is less than half of the hole deformation potential and (ii) most of the electrons will be in the L valley, which has a smaller effective mass than the heavy-hole band.[27] Broadening and shifting of cw Raman spectra in p- and n-type doped Ge provide empirical evidence in support of the comparatively minor impact of intra-L-valley SPE's on the LO phonon self-energy.[4,5,28] Although SPE's explain the spectra of p-type doped Ge,[5] the n-type doped Ge spectral features are attributed to phonon confinement effects rather than intra-L-valley SPE's.[4,27]

The SPE's that contribute substantially to the LO phonon self-energy are intra-heavy-hole–valence-band transitions and inter-heavy-hole$\leftrightarrow$light-hole transitions. These contributions are derived separately in the Appendixes; the total density of states and energy shift are sums of the separate contributions. (Intraband transitions within the light and split-off valence bands can be neglected since the effective masses, and therefore the densities of states, of these bands are much smaller than that of the heavy-hole valence band.[28] Interband transitions involving the split-off valence band can also be neglected since the required transition energies are much larger than the LO phonon energies.) The SPE calculations use Fermi-Dirac statistics, a parabolic heavy-hole band, and a nonparabolic light-hole band.

To determine the broadening of the LO phonons probed by the experiments, the expressions for ρ_{intra} and ρ_{inter} given in the Appendixes are added and evaluated using $E = E_{q_0}$ and $q = q_0$. The LO phonon line broadening shown in Fig. 1 for various hole temperatures (T_H) illustrates that, in general, the LO phonon linewidth increases with increasing N. For the hole temperature produced in the experiments

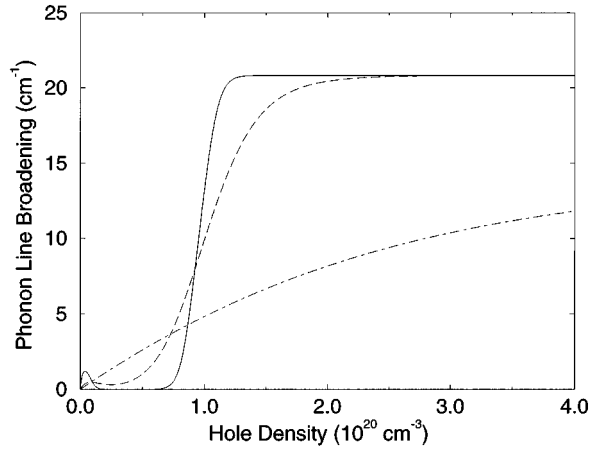

FIG. 1. Dependence of the LO phonon line broadening on hole density for hole temperatures of 77 K (solid line), 300 K (dashed line), and 3000 K (dot-dashed line).

[T_H=3000 K (Ref. 22)], the linewidth increases sublinearly with N and more than 99% of the line broadening can be attributed to intra-heavy-hole transitions. The structure in the 77 K and 300 K line broadening at low carrier densities ($N<5\times10^{19}$ cm^{-3}) is caused by inter-heavy-hole $\leftrightarrow$light-hole transitions; for higher N and T_H, the contribution of inter-heavy-hole$\leftrightarrow$light-hole transitions to the line broadening is negligible.

Figure 2 shows the total phonon energy shift as a function of N for $E=E_{q_0}$, $q=q_0$ phonons. With increasing N, the general trend is a reduction in phonon energy for all T_H due to the contribution of inter-heavy-hole$\leftrightarrow$light-hole SPE's. For T_H=3000 K, the contribution of inter-heavy-hole $\leftrightarrow$light-hole SPE's dominates the contribution of intra-heavy-hole SPEs, thereby giving a sublinear increase in the magnitude of the LO phonon energy shift with increasing N.

For cooled holes, the LO phonon linewidth increase and energy shift depend on phonon wave vector, through the dependence of ρ_{intra} on q; these predictions are qualitatively consistent with Olego and Cardona's observations of a dependence of Raman line broadening and shifting on excitation wavelength in extrinsic Ge, at temperatures of 77 K and 300 K.[5] However, for hot holes, the line broadening and shifting dependence on phonon wave vector is negligible.

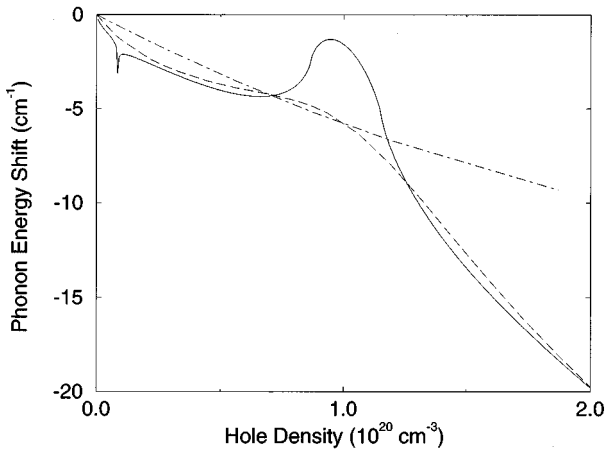

FIG. 2. Dependence of the total LO phonon energy shift on hole density for hole temperatures of 0 K (solid line), 300 K (dashed line), and 3000 K (dot-dashed line).

B. Model for coupled carrier and phonon dynamics

To determine the temporal evolution of the LO phonon occupation number (n_q) produced by an intense picosecond light pulse, ODYK's low excitation ($N<10^{18}$ cm^{-3}) model for coupled carrier-phonon dynamics[12] is modified. Our extended model addresses the high-excitation regime and includes the increased likelihood of nonequilibrium LO phonon reabsorption by free carriers as N increases, as well as the increased anharmonic decay rate of LO phonons as the lattice temperature increases. Both processes limit the attainable LO phonon occupation number in the high-excitation regime. Since this low-excitation regime model has been described in detail elsewhere,[12] this section gives only a brief description of the modifications made to describe high excitations; these modifications all involve its description of LO phonon dynamics.

For both high and low excitations, n_q is given by the rate equation

$$\frac{\partial n_q}{\partial t}=\left[\frac{\partial n_q}{\partial t}\right]_{\text{gen}}^{\text{tot}}-\Gamma(n_q-n_q^{\text{eq}}). \tag{6}$$

The second term describes anharmonic decay of the nonequilibrium LO phonons; both n_q^{eq}, the equilibrium phonon occupation number, and Γ, the LO phonon anharmonic decay rate, are calculated as functions of the steady-state lattice temperature (T_L). The first term is the net generation rate of phonons, which includes nonequilibrium phonon emission and absorption through carrier transitions. The ''tot'' indicates that this is the sum of the net generation terms associated with intra-L-valley electron and intra-heavy-hole valence-band hole transitions, each of which has the form

$$\begin{aligned}\left[\frac{\partial n_q}{\partial t}\right]_{\text{gen}}=&\frac{\hbar D_c^2}{4\pi^2\tilde{\rho}E_q}\int d^3k f_{\vec{k}}[(n_q+1)(1-f_{\vec{k}-\vec{q}})\\&\times\delta(E(\vec{k})-E(\vec{k}-\vec{q})-E_q)-n_q(1-f_{\vec{k}+\vec{q}})\\&\times\delta(E(\vec{k}+\vec{q})-E(\vec{k})-E_q)].\end{aligned} \tag{7}$$

The first and second terms of the integrand describe nonequilibrium LO phonon emission and absorption respectively. $E(\vec{k})$ are carrier energies and the $f_{\vec{k}}$ functions describe the carrier distributions. Just as hole transitions within the heavy-hole valence band dominate over electron transitions in the L-valley as contributors to the LO phonon self-energy, $\sim$ 95% of nonequilibrium LO phonons in photoexcited Ge are generated through hole cooling.[29] Inter-heavy-hole $\leftrightarrow$light-hole transitions are not considered in either the low- or high-excitation models; this omission is justified by the phonon self-energy calculations in Sec. III A, which show that the density of states for these processes is negligible for the LO phonon wave vector probed by the experiments.

To simplify Eq. (6) we assume (i) empty final states for carriers undergoing both excitation and deexcitation

$([1-f_{\vec{k}\pm\vec{q}}]\approx 1)$ and (ii) Maxwell-Boltzmann statistics for the carrier distributions. This gives

$$\frac{\partial n_q}{\partial t} = AN(n_q+1) - BNn_q - \Gamma(n_q - n_q^{\mathrm{eq}}). \tag{8}$$

The factors A and B are analytical functions of T_H, E_q, q, m_h, $\tilde{\rho}$, and D_c.[22] ODYK's low excitation model applied the further approximation that $n_q \approx n_q^{\mathrm{eq}}$ in the phonon emission $[\propto N(n_q+1)]$ and phonon absorption $(\propto Nn_q)$ terms in Eq. (8).[29] This approximation is unapplicable in the high-excitation regime since substantial nonequilibrium LO phonon populations are generated. Furthermore, it is equivalent to the untenable assumption that the LO phonon lifetime is unaffected by SPE's; to see this, note that both $N(n_q+1)$ and Nn_q increase as N and n_q increase, but in combination they predict a sublinear increase in the *net generation rate* of nonequilibrium LO phonons. This is qualitatively consistent with the SPE-induced phonon lifetime reduction predicted above by the phonon self-energy model and with previous discussions of the competing roles of phonon emission and reabsorption in the cooling of photoexcited carriers (i.e., the hot phonon effect).[15,17]

The *effective LO phonon decay rate* Γ' in the presence of N photoexcited carriers can be determined by writing $n_q = n_q^{\mathrm{eq}} + \delta n_q$ and by rewriting Eq. (8) as

$$\frac{\partial \delta n_q}{\partial t} = AN(n_q^{\mathrm{eq}}+1) - BNn_q^{\mathrm{eq}} - \Gamma' \delta n_q, \tag{9}$$

where

$$\Gamma' = \Gamma + (B-A)N. \tag{10}$$

The first and second terms of Eq. (9) describe nonequilibrium LO phonon emission and absorption, driven by the temperature difference between the photo-excited holes and the lattice; these terms cancel each other in the limit $T_c \rightarrow T_L$. The above definition of Γ' is chosen because the $(B-A)N$ term contains the same physics as the contribution of intra-heavy-hole transitions to the imaginary part of the LO phonon self-energy [see Eqs. (4) and (A1)].

IV. RESULTS AND DISCUSSION

A. Phonon self-energy

Figure 3 shows typical time-averaged anti-Stokes spectra produced by low- and high-fluence light pulses which illustrate that with increasing N (i) the Raman lines are asymmetrically broadened along their low-frequency sides and shifted to lower frequencies and (ii) the integrated intensity of the Raman line increases along with n. These features are qualitatively consistent with those of simulations based on the theories presented in Sec. III.

Figure 4(a) illustrates a weakly sublinear increase in anti-Stokes FWHM with increasing N for intrinsic Ge. For fits to this and other data sets of the form N^{γ}, γ is typically 0.74 $\pm$ 0.12. Similar results are obtained for the p-type doped samples. Figure 4(a) also shows a simulation for which the linewidth increase is roughly proportional to N^{γ}, where $\gamma = 0.83$. The simulations include phonon line broadening due to (i) SPE's involving N photoexcited holes with $T_H =$ 3000 K, (ii) SPE's involving N_a holes in the doped samples with $T_H = 300$ K, and (iii) the small increase in steady-state lattice temperature with increasing fluence. Note that the simulations are relatively insensitive to whether or not the doping-induced holes are considered to be cold or hot. The anharmonic contribution is minor ($< 10\%$) and approximately linear[30] for the range of lattice temperatures produced in the experiments [300–350 K (Ref. 31)]. In principle, there may be additional linewidth contributions due to dephasing events or inhomogeneous line-broadening processes, but these are not included in the simulations. Nevertheless, the data and simulations agree, both qualitatively and quantitatively, within experimental error.

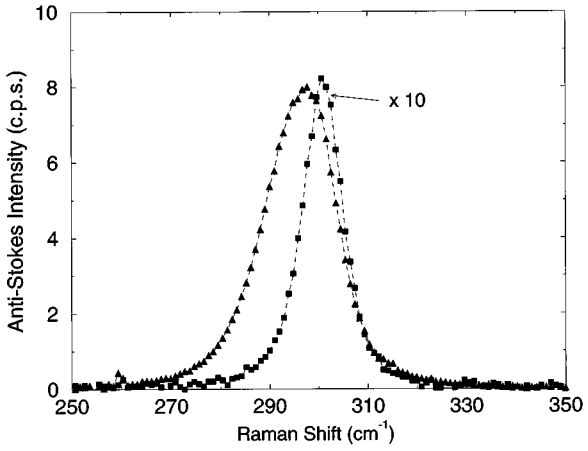

FIG. 3. Measured anti-Stokes spectra with background subtracted. The $N = 2\times10^{19}$ cm^{-3} spectrum (squares) has been multiplied by 10 to facilitate comparison to the $N = 1.5\times10^{20}$ cm^{-3} spectrum (triangles). The Raman line shift is measured relative to the laser line. The dotted lines are guides to the eye.

Because the observed Raman line broadening can be primarily attributed to a reduction in phonon lifetime, the anti-Stokes linewidth increase can be used as a measure of the

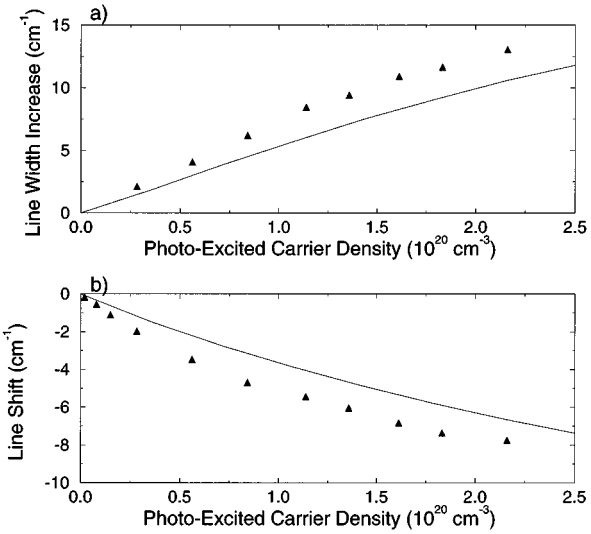

FIG. 4. Dependence of the time-integrated anti-Stokes Raman (a) linewidth increase and (b) line shift on photoexcited carrier density. The data sets (triangles) are simulated by the solid lines using $2\Gamma_0 = 12$ cm^{-1}.

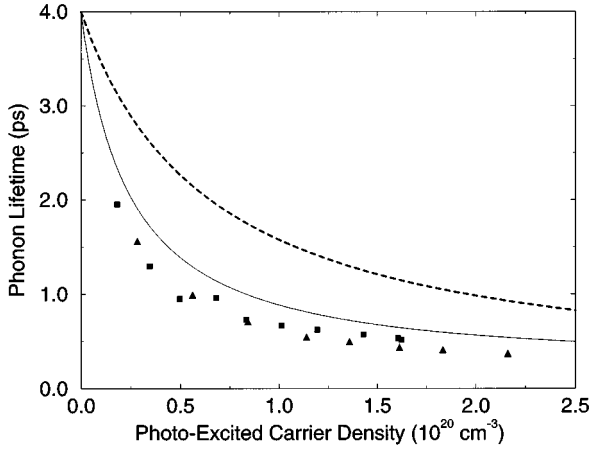

FIG. 5. Measured (squares and triangles) and simulated (solid line, self-energy model; dashed line, coupled carrier-phonon dynamics model) dependence of the temporal and spatial average of the phonon lifetime on photoexcited carrier density. The filled triangles correspond to the intrinsic Ge data set in Fig. 4(a)

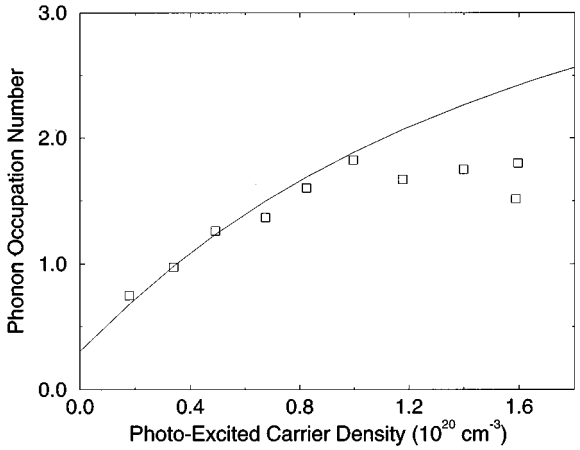

FIG. 6. Dependence of the measured (squares) and simulated (solid line) time-integrated phonon occupation number on photoexcited carrier density.

lower limit of the phonon lifetime. Figure 5 shows the dependence of the spatially and temporally averaged phonon lifetime on N in intrinsic Ge, as given by two data sets. Note that spatial-temporal convolution effects cause the data-derived phonon lifetime to be underestimated by $\sim$ 10%. Figure 5 also shows the results of a calculation of the phonon lifetime dependence on N, which includes the influences of both SPE's and steady-state lattice heating. The agreement between the data and simulation is well within experimental error. Both the data and calculation show a reduction in phonon lifetime from 4 ps (Ref. 12) to $\sim$ 0.5 ps, for an increase in N to 2×10^{20} cm^{-3}. According to the phonon self-energy theory of Sec. III, nearly all of this lifetime reduction can be attributed to *intra-heavy-hole* valence-band SPE's rather than inter-heavy-hole$\leftrightarrow$light-hole SPEs or steady-state lattice heating.

Figure 4(b) shows the measured and simulated (with $T_H=3000$ K) dependence of the anti-Stokes Raman line shift on N for intrinsic Ge. Similar results are obtained for the p-type doped Ge samples. The line shifts are negative and their magnitudes increase sublinearly with N. Numerical fits, of the form $-N^{\gamma}$, to the data and to the simulations give $\gamma=0.68\pm0.19$ and $\gamma=0.76$, respectively. Taking convolution effects into account, for an increase in N to 2×10^{20} cm^{-3}, the phonon frequency is reduced by $\sim$8 cm^{-1}. For both intrinsic and p-type doped Ge, the degree of agreement between each data set and its simulation is well within experimental error. According to the simulations, the majority of the Raman line shift can be attributed to the phonon frequency shift caused by SPE's; lattice heating accounts for $<$ 15% of the observed line shift. Furthermore, the contribution of *inter-heavy-hole$\leftrightarrow$light-hole* SPE's to the line shift dominates over that of intra-heavy-hole SPE's.

Both the observed and simulated Raman lines become asymmetically broadened along their low-frequency sides as N increases. The exclusive source of the asymmetry in the *simulated* Raman lines is spatial-temporal convolution. The degree of agreement between the measured and simulated Raman lineshapes suggests that convolution effects may be responsible for the majority of the asymmetry of the measured high-N Raman lines. This does not preclude the possible role of a Fano interaction between the phonons and a continuum of electronic excitations.[5] However, in the absence of a detailed model of the Fano-interference effect in photoexcited Ge, this effect is not examined further.

B. Time-integrated and time-resolved phonon dynamics

Figure 6 shows $n(N)$, based on measured time-integrated Stokes and anti-Stokes intensities, and on Eq. (1) with $Q=1$. The key feature of the $n(N)$ data is the sublinear increase in n with increasing N. The Raman intensities were also used to calculate time-integrated Raman scattering cross sections using Eq. (3). With $N>10^{20}$ cm^{-3}, the cross section is reduced by as much as 30% relative to the low-excitation cross section. Since the laser frequency is below the frequency of the Raman resonance peak, this reduction is qualitatively consistent with measured cw Raman resonance profiles of extrinsic Ge.[24,25]

Figure 7 shows the time-resolved Stokes and anti-Stokes intensities for $N=8\times10^{19}$ cm^{-3}. The inset shows the time-resolved anti-Stokes intensity produced by 20$\times$ weaker, 4-ps pump and probe pulses with a 76-MHz repetition rate.[12] Under both high and low excitations, there is a rapid increase in scattered light intensity associated with phonon generation by cooling photoexcited carriers. The striking difference between the high- and low-excitation data is the rapid drop in the high-excitation Raman intensity at $t>0$ to below that of the background intensity. (The background Raman intensity, given by averaging the measured signals at $t\leqslant-10$ ps, is indicated by the solid horizontal line.) Equation (3) was used to calculate the temporal evolution of the cross section, measured relative to the average cross section at $t\leqslant-10$ ps. A cross section reduction of $\sim$ 15% at $t>0$ is found, which accounts for part of the drop in signal.

Figure 8 shows $n(t)$, derived from the Raman intensities shown in Fig. 7 using Eq. (1) with $Q=1$. There are three features of the $n(t)$ data to note. First, the temporal peak occurs sooner than at low excitations. Second, n is less than half of that predicted by a linear extrapolation of predicted

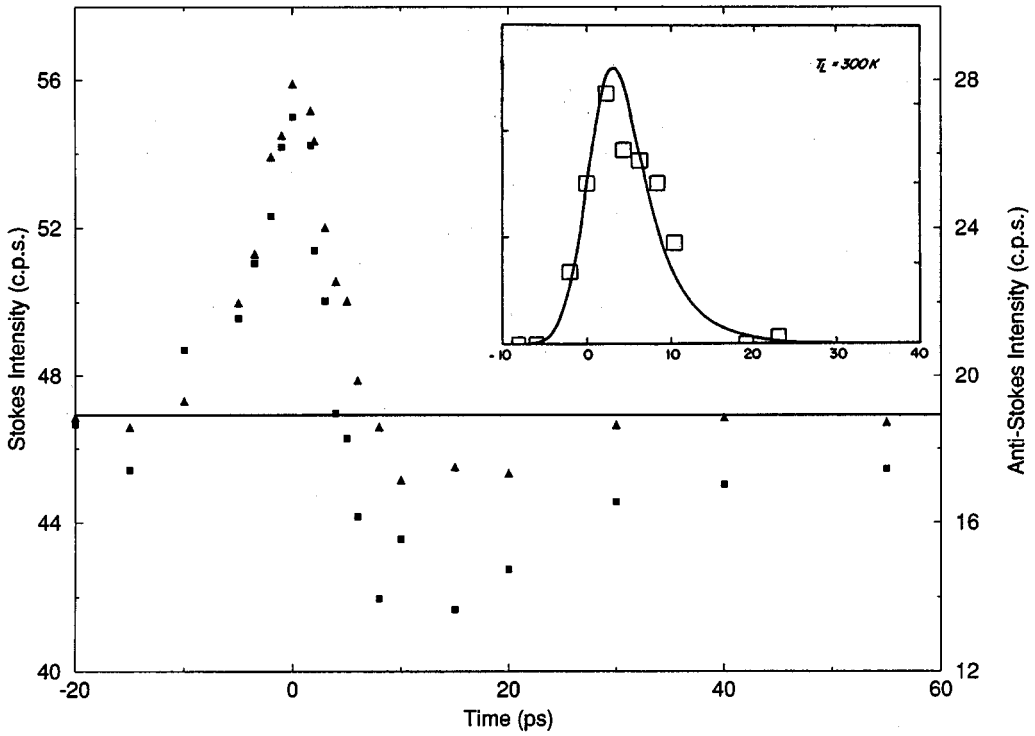

FIG. 7. Temporal evolution of measured Stokes (filled squares) and anti-Stokes (filled triangles) Raman intensities with $N=8\times10^{19}$ cm^{-3}. The inset [from ODYK (Ref. 12)] shows the measured anti-Stokes Raman intensity (empty squares) produced by excitation with $20\times$ weaker light pulses. The solid line in the inset represents the temporal evolution of the phonon occupation number given by ODYK's low excitation phonon dynamics model (Ref. 12).

phonon occupation numbers under low excitations. This feature is consistent with the sublinearity of $n(N)$ shown in Fig. 6. Third, at $t>0$, $n(t)$ is greater than the background occupation number; this indicates that the reductions in scattered light intensity, at $t>0$ in Fig. 7, cannot be attributed to a reduction in the probe generated phonon population due to the presence of pump generated carriers.

There are a number of processes that could play a role in limiting the phonon population produced by a train of high-fluence light pulses and contribute to the sublinearity in $n(N)$, as evidenced by both the time-integrated and time-resolved data. As discussed previously, both SPE's and lattice heating can reduce the phonon lifetime and the phonon population. Another possibility is that, under conditions of carrier degeneracy, holes would emit fewer phonons. (Because most of the phonons are generated by hole cooling,[12] conduction-band filling need not be considered.) Bleaching of the electronic transitions could also lead to the sublinearity of $n(N)$; however, bleaching effects can be neglected under our excitation conditions.

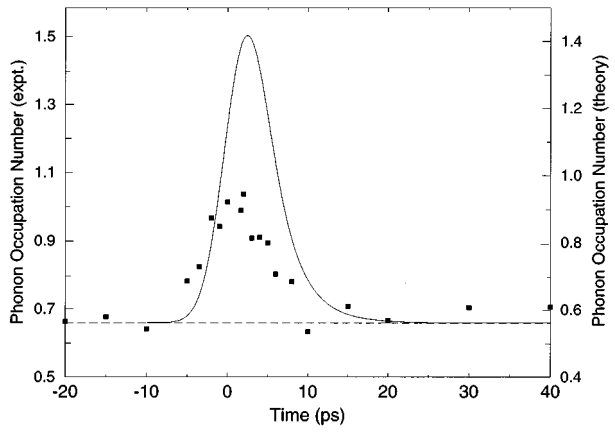

FIG. 8. Temporal evolution of the measured (squares) and simulated (solid line) phonon occupation number corresponding to the data in Fig. 7. The dashed line represents the background phonon occupation number for both the data and the simulation. The scales for the data and the simulation are the same, but offset by the difference between the measured and simulated backgrounds.

We suggest that the sublinearity in $n(N)$ and shift towards $t=0$ of the temporal peak in $n(t)$ can be attributed primarily to a SPE-induced reduction in phonon lifetime. Figures 6 and 8 include simulations of $n(N)$ and $n(t)$ based on the carrier-phonon dynamics model, which include the minor but non-negligible influence of steady-state lattice heating on the phonon lifetime. (Neglect of lattice heating causes n to be overestimated by $\sim$ 10% for $N=2\times10^{20}$ cm^{-3}.) The $n(N)$ simulation predicts a sublinear increase in n with increasing N, in qualitative agreement with the data. However, the simulation overestimates $n(N)$, especially for $N>10^{20}$ cm^{-3}. The simulations of $n(t)$ are also qualitatively similar to the data and predict a shift in the temporal peak of $n(t)$ towards $t=0$ as N is increased. However, the temporal peak in the measured $n(t)$ occurs earlier than the peak of the simulation of $n(t)$ by $\sim$ 1 ps, and as for $n(N)$, the simulation overestimates the phonon occupation number. These discrepancies may be related to the following assumptions.

(i) The first assumption is that Q is constant over the full range of carrier densities produced in the experiments. Con-

tinuous wave measurements of Raman scattering cross sections in p-type doped Ge suggest that σ_{AS}/σ_S is reduced by $\sim$ 5% for $N_a=4\times10^{19}$ cm^{-3}.[25] If a high density of hot carriers also reduces Q, then the $n(N)$ (at large N) and $n(t)$ data (especially near $t=2$ ps when N is maximized) will be underestimated. For example, a decrease in Q of only 10%, for an increase in N to 1.6×10^{20} cm^{-3}, would be sufficient to bring the $n(N)$ data and simulations into agreement.

(ii) There are the simplifying assumptions in the phonon dynamics model. Figure 5 includes a comparison of the N dependence of the effective phonon lifetime predicted by the carrer-phonon dynamics model to that predicted by the phonon self-energy model. This figure illustrates that the carrier-phonon dynamics model overestimates the high-N phonon lifetime by as much as $2\times$ for $N=2\times10^{20}$ cm^{-3}. The discrepancy can be traced to the assumption of empty final hole states [in Eq. (7)], which leads to an overestimate of both A and B in Eq. (8). Since the error in A is larger, this leads to an underestimate of Γ' in Eq. (10), which is compounded by the adoption of Maxwell-Boltzmann statistics. The overestimate of the phonon lifetime causes the simulations to overestimate $n(N)$ and $n(t)$ and predict that $n(t)$ peaks at larger time delays.

In combination, these limitations to the data analysis and the phonon dynamics model should be sufficient to account for the discrepancies between the measurements and simulations of the phonon occupation number. Despite these limitations, reasonable agreement exists between the data and simulations, well within (i) the systematic error in measuring n (due to the uncertainty in Q) (ii) the error in calculating n associated with the uncertainties in the pump and probe fluences; and (iii) the experimental error in $t=0$ of $\pm$ 1 ps. The extent of the agreement is gratifying considering that no fitting parameters were used in the simulations.

V. CONCLUSIONS

Nonequilibrium phonon populations and the phonon self-energy in strongly photo-excited intrinsic and p-type doped germanium have been studied using time-resolved Raman-scattering intensity measurements on a picosecond time scale and time-integrated, simultaneous measurements of Raman linewidths, line shifts, and intensities. The time-integrated measurements show asymmetric broadening and shifting of the Raman lines, a sublinear increase in the phonon occupation number, and a reduction in the Raman-scattering cross section with increasing N. The time-resolved experiments reveal a shift in the temporal peak of the phonon occupation number with increasing N and a transient reduction in the Raman-scattering cross section. Phonon self-energy calculations indicate that the phonon lifetime reduction is consistent with primarily intra-heavy-hole SPE's, while the reduction in phonon frequency, which manifests itself in shifting of the Raman lines, is consistent with primarily inter-heavy-hole $\leftrightarrow$light-hole SPE's. The role of holes in affecting phonon lifetimes in Ge is similar to that which has been identified in GaAs.[20] Calculations using coupled phonon and carrier kinetics show that most of the sublinearity of $n(N)$ and shift in the temporal peak of the phonon occupation number can be accounted for by considering the increased probability of nonequilibrium phonon reabsorption through intraband SPE's due to the presence of high carrier densities.

Together our frequency-domain studies of the phonon self-energy and time-domain studies of nonequilibrium phonon populations in photoexcited Ge self-consistently reveal the importance of hole SPE's in renormalizing the phonon frequency and reducing the phonon lifetime. For $N=2\times10^{20}$ cm^{-3}, the measured phonon lifetime is reduced to $\sim$ 0.5 ps from the low-excitation lifetime of 4 ps and the phonon frequency is reduced by $\sim$ 8 cm^{-1}.

ACKNOWLEDGMENTS

We thank Professor Jeff Young, of the University of British Columbia, for helpful discussions. We are grateful to M. Stutzman, H.P. Weber, and M. Cardona, of the Max Planck Institut für Festkörperforschung, for providing the p-type doped Ge samples. This work was supported by the Natural Sciences and Engineering Research Council of Canada and the Ontario Laser and Lightwave Research Center.

APPENDIX A: INTRABAND DENSITY OF STATES

For a general hole transition energy E, the density of intra-heavy-hole SPEs is given by

$$\rho_{\text{intra}}(E,q)=\frac{1}{4\pi^3}\int d^3k f_{h,\vec{k}} \times[(1-f_{h,\vec{k}+\vec{q}})\,\delta(E_h(\vec{k}+\vec{q})-E_h(\vec{k})-E) -(1-f_{h,\vec{k}-\vec{q}})\,\delta(E_h(\vec{k})-E_h(\vec{k}-\vec{q})-E)]. \tag{A1}$$

The first and second δ-function terms describe hole excitation and relaxation processes, respectively. The dependence of ρ_{intra} on N and T_H is contained in f_h and $(1-f_h)$, the occupation probabilities of the initial and final heavy-hole states. $E_h(k)=\hbar^2k^2/2m_h$ is the energy of a heavy hole with effective mass m_h.

The integral is completed analytically using a method similar to that of Young and Kelly[32] and Fermi-Dirac statistics to obtain

$$\rho_{\text{intra}}(E,q)=\frac{m_h^2}{2\pi^2\hbar^4q}\left[E+k_BT_H\ln\left(\frac{\exp(x_+)+\exp(\eta)}{\exp(x_-)+\exp(\eta)}\right)\right], \tag{A2}$$

where

$$x_\pm=\frac{\hbar^2S_\pm^2}{2m_hq^2}\frac{1}{k_BT_H},\quad S_\pm=\frac{m_hE}{\hbar^2}\pm\frac{q^2}{2}, \tag{A3}$$

and $\eta=E_F/k_BT_H$, the reduced Fermi energy, is determined according to N and T_H using Nilsson's approximation.[33]

For a system at $T=0$, $\rho_{\text{intra}}(E,q)$ includes all transitions from filled electronic states below the Fermi energy to empty states above the Fermi energy and Eq. (A2) reduces to

$$\rho_{\text{intra}}(E,q)=\begin{cases}\dfrac{m_h^2}{2\pi^2\hbar^4 q}E & \text{for} \quad E\leqslant E_- \\ \dfrac{m_h^2}{2\pi^2\hbar^4 q}\left[E_F-\dfrac{\hbar^2}{2m_h}\dfrac{S_+^2}{q^2}\right] & \text{for} \quad E_-\leqslant E\leqslant E_+ \\ 0 \quad \text{for} \quad E\geqslant E_+, \end{cases} \tag{A4}$$

where $E_\pm=\hbar^2/2m_h(2k_Fq\pm q^2)$ and k_F is the Fermi wave vector.

APPENDIX B: INTERBAND DENSITY OF STATES

The density of hole transitions between the heavy- and light-hole valence bands, with transition energy E, is

$$\begin{aligned}\rho_{\text{inter}}(E,q)=&\frac{1}{4\pi^3}\int d^3k f_{h,\vec{k}} \\ &\times[(1-f_{l,\vec{k}+\vec{q}})\,\delta(E_l(\vec{k}+\vec{q})-E_h(\vec{k})-E) \\ &-(1-f_{l,\vec{k}-\vec{q}})\,\delta(E_h(\vec{k})-E_l(\vec{k}-\vec{q})-E)] \\ &+f_{l,\vec{k}}[(1-f_{h,\vec{k}+\vec{q}})\,\delta(E_h(\vec{k}+\vec{q})-E_l(\vec{k})-E) \\ &-(1-f_{h,\vec{k}-\vec{q}})\,\delta(E_l(\vec{k})-E_h(\vec{k}-\vec{q})-E)]. \end{aligned} \tag{B1}$$

The first two δ-function terms describe hole excitation and relaxation processes for which the initial state is in the heavy-hole band. The second two δ-function terms describe hole excitation and relaxation processes for which the initial state is in the light-hole band. The dependence of ρ_{inter} on N and T_H is contained in the functions f_h, f_l, the occupation probabilities for the heavy- and light-hole bands. E_l is the energy of a hole in the nonparabolic light-hole band with near zone-center effective mass m_l,

$$E_l(\vec{k})=\left[\varepsilon_1+\frac{\hbar^2k^2}{2m_h}\right]\left[1-\exp\left(\frac{-\hbar^2k^2}{2m_l}\frac{1}{\varepsilon_2}\right)\right], \tag{B2}$$

where $\varepsilon_1=169.8$ meV and $\varepsilon_2=175.4$ meV. It is essential to address the nonparabolicity of the light-hole band since the parabolic band approximation leads to the unphysical situation of a finite density of states for infinite interband transition energies. Equation (B2) is a numerical fit to Kane's[34] light-hole band, which describes the asymptotic increase of the light-hole effective mass towards that of the heavy-hole band with increasing k. This description is preferable to, for example, the analytical form of Conwell and Vassel,[35] which allows the heavy-hole and light-hole bands to cross at large k.

The integral in Eq. (B1) is greatly simplified by assuming that $\vec{q}=\vec{0}$ or that only direct transitions are allowed. Then only the first and fourth δ-function terms in Eq. (B1) need to be kept to obtain, with simplification,

$$\rho_{\text{inter}}(E)=\frac{1}{4\pi^3}\int d^3k[f_{h,k}-f_{l,k}]\,\delta(R), \tag{B3}$$

where $R\equiv E_l(k)-E_h(k)-E$. The δ function can be rewritten using $\delta(R)=\delta(k-\tilde{k})/|\partial R/\partial k|$, where $\tilde{k}$ is the solution to $R=0$. Due to the nonparabolicity of the light-hole band, $\tilde{k}$ is determined numerically. With the definition $\tilde{E}\equiv\hbar^2\tilde{k}^2/2m_h$, an analytical expression for a fit to the numerical solution is given by

$$\tilde{E}(E)=-\epsilon\varepsilon_3\ln\frac{\varepsilon_1-E}{\varepsilon_1} \quad \text{for} \quad 0\leqslant E\leqslant\varepsilon_1, \tag{B4}$$

where $\varepsilon_3\equiv\varepsilon_2 m_l/m_h$ and $\epsilon=-2/\ln\varepsilon_1$ (with ε_1 in units of eV) are positive constants dictated by the curvatures of the heavy- and light-hole bands.

The final form of the density of inter-heavy-hole $\leftrightarrow$light-hole transitions is

$$\rho_{\text{inter}}(E)=\frac{m_h^{3/2}(2\tilde{E})^{1/2}}{\pi^2\hbar^3}\frac{\exp\tilde{E}/\varepsilon_3}{\varepsilon_4+\tilde{E}/\varepsilon_3}[f_h(\tilde{E})-f_l(\tilde{E}+E)] \quad \text{for} \quad 0\leqslant E\leqslant\varepsilon_1, \tag{B5}$$

where $\varepsilon_4\equiv(\varepsilon_1/\varepsilon_2)(m_h/m_l)-1$. Note that as E approaches the maximum allowed transition energy ε_1, both $\tilde{E}$ and $\rho_{\text{inter}}/[f_h(\tilde{E})-f_l(\tilde{E}+E)]$ diverge. If $[f_h(\tilde{E})-f_l(\tilde{E}+E)]$ is nonzero, this can cause ρ_{inter} to diverge. In general, ρ_{inter} is dominated by this divergence. Since $f_h(\tilde{E})$ and $f_l(\tilde{E}+E)$ become small as $\tilde{E}\to\infty$, the lower T_H, the weaker the divergence in ρ_{inter}. The behavior of ρ_{inter} for $E=E_{q_0}$, and $N<1\times10^{19}$ cm^{-3} is of note because this is the only range of hole densities for which ρ_{inter} is significant compared to ρ_{intra}; here ρ_{inter} decreases with increasing T_H. For higher N and all T_H, ρ_{inter} at $E=E_{q_0}$ is much smaller than ρ_{intra} ($\sim$ 1–10%). For a system at $T=0$, only hole excitation transitions from the heavy-hole to the light-hole band are possible:

$$\rho_{\text{inter}}(E)=\begin{cases}\dfrac{m_h^{3/2}(2\tilde{E})^{1/2}}{\pi^2\hbar^3}\dfrac{\exp(\tilde{E}/\varepsilon_3)}{\varepsilon_4+\tilde{E}/\varepsilon_3} & \text{for} \quad \tilde{E}\leqslant E_F\leqslant\tilde{E}+E \\ 0 \quad \text{for} \quad E_F<\tilde{E};\tilde{E}+E<E_F. \end{cases} \tag{B6}$$

APPENDIX C: PHONON ENERGY SHIFT

The contributions of intra- and inter-valence-band transitions to the LO phonon energy shift are calculated separately using the forms of ρ_{intra} and ρ_{inter} given above, evaluated at $E=E_q$. For $T_H>0$, the Hilbert transform [see Eq. (5)] of ρ_{intra} is calculated numerically; however, for $T_H=0$, an analytical expression can be obtained to give

$$\begin{aligned}\Delta E_{q,\text{intra}}(E_q,q)=&\frac{D_H^2\hbar}{4\pi\tilde{\rho}cE_q}\frac{m_h^2}{2\pi^2\hbar^4q}\left\{\left(E_F-\frac{\hbar^2}{2m_h}\frac{S_+^2}{q^2}\right)\right. \\ &\times\ln\left[\frac{E_++E_q-\hbar^2q^2/m_h}{|E_+-E_q|}\right]+\left(E_F-\frac{\hbar^2}{2m_h}\frac{S_-^2}{q^2}\right) \\ &\left.\times\ln\left[\frac{|E_+-E_q-\hbar^2q^2/m_h|}{E_++E_q}\right]+\frac{\hbar^2q^2}{2m_h}-E_+\right\}, \end{aligned} \tag{C1}$$

where E_+ and $S_\pm$ are as given above. The intraband energy shift is negative for most N and T_H; at low temperatures with $N<2.5\times10^{20}$ cm^{-3}, the shift is positive.

The Hilbert transform of ρ_{inter} is calculated numerically. For all N and T_H the interband LO phonon energy shift is negative, increases sublinearly in magnitude as N increases, and decreases in magnitude as T_H increases. There is some structure in the $T_H=0$ energy shift, near $N=1\times10^{19}$ cm^{-3}, associated with a pole in the Hilbert transform integrand that occurs when $\rho_{\text{inter}}(E_q)\neq0$. As T_H increases, $\rho_{\text{inter}}(E_q)$ decreases and the structure in the energy shift associated with this pole is smoothed out.

[1] T.R. Hart, R.L. Aggarwal, and B. Lax, Phys. Rev. B **1**, 638 (1970).

[2] F. Cerdeira, W. Dreybrodt, and M. Cardona, Solid State Commun. **10**, 591 (1972).

[3] J. Menéndez and M. Cardona, Phys. Rev. B **29**, 2051 (1984).

[4] F. Cerdeira and M. Cardona, Phys. Rev. B **5**, 1440 (1972).

[5] D. Olego and M. Cardona, Phys. Rev. B **23**, 6592 (1981).

[6] G. Contreras, A.K. Sood, M. Cardona, and A. Compaan, Solid State Commun. **49**, 303 (1984).

[7] D. von der Linde, J. Kuhl, and H. Klingenberg, Phys. Rev. Lett. **44**, 1505 (1980).

[8] J.A. Kash, J.C. Tsang, and J.M. Hvam, Phys. Rev. Lett. **54**, 2151 (1985).

[9] J.A. Kash, S.S. Jha, and J.C. Tsang, Phys. Rev. Lett. **58**, 1869 (1987).

[10] J.F. Young, K. Wan, and H.M. van Driel, Solid-State Electron. **31**, 455 (1988).

[11] A.Z. Genack, L. Ye, and C.B. Roxlo, in SPIE **942**, 130 (1988); L. Ye, C.B. Roxlo, and A.Z. Genack, Bull. Am. Phys. Soc. **32**, 934 (1987).

[12] A. Othonos, H.M. van Driel, J.F. Young, and P.J. Kelly, Phys. Rev. B **43**, 6682 (1991).

[13] H.D. Fuchs, C.H. Grein, R.I. Devlen, J. Kuhl, and M. Cardona, Phys. Rev. B **44**, 8633 (1991).

[14] J.F. Young, D.J. Lockwood, J.M. Baribeau, P.J. Kelly, A. Othonos, and H. M. van Driel, in *Light Scattering in Semiconductor Structures and Superlattices*, edited by D.J. Lockwood and J.F. Young (Plenum, New York, 1991), p. 401.

[15] H.M. van Driel, Phys. Rev. B **19**, 5928 (1979).

[16] W. Pötz and P. Kocevar, Phys. Rev. B **28**, 7040 (1983).

[17] A. Compaan, M.C. Lee, and G.J. Trott, Phys. Rev. B **32**, 6731 (1985).

[18] *Hot Carriers in Semiconductor Nanostructures; Physics and Applications*, edited by J. Shah (Academic Boston, 1992).

[19] J.A. Kash and J.C. Tsang, in *Light Scattering in Solids VI*, edited by M. Cardona and G. Güntherodt (Springer-Verlag, Berlin, 1991), p. 423.

[20] P. Brockmann, J.F. Young, P. Hawrylak, and H.M. van Driel, Phys. Rev. B **48**, 11 423 (1993).

[21] M.L. Ledgerwood and H.M. van Driel, Bull. Am. Phys. Soc. **38**, 808 (1993).

[22] M.L. Ledgerwood, J.F. Young, and H.M. van Driel, Solid State Commun. **89**, 789 (1994).

[23] M.L. Ledgerwood, Ph.D. thesis, University of Toronto, 1995 (unpublished).

[24] A.K. Sood, G. Contreras, and M. Cardona, Phys. Rev. B **31**, 3760 (1985).

[25] M.I. Alonso and M. Cardona, Phys. Rev. B **37**, 10 107 (1988).

[26] G. Abstreiter, M. Cardona, and A. Pinczuk, in *Light Scattering in Solids IV*, edited by M. Cardona and G. Güntherodt (Springer-Verlag, Berlin, 1984), p. 5.

[27] R.N. Dexter, H.J. Zeiger, and B. Lax, Phys. Rev. B **104**, 637 (1956); M. Neuberger, *Handbook of Electronic Materials, Group IV Semiconducting Materials* (IFI/Plenum, New York, 1971), Vol. 5; G. Gagliani and L. Reggiani, Nuovo Cimento **30**, 207 (1975); in *Numerical Data and Functional Relationships in Science and Technology*, edited by O. Madelung, Landolt-Börnstein, New Series, Group III, Vol. 17, Pt. a (Springer-Verlag, Berlin, 1982); L. Reggiani, in Proceedings of the 15th International Conference on the Physics of Semiconductors, Kyoto [J. Phys. Soc. Jpn. Suppl. A **49**, 317 (1980)]. R. Brunetti, C. Jacoboni, F. Nava, L. Reggiani, G. Bosman, and R.J. Zijlstra, J. Appl. Phys. **52**, 6713 (1981).

[28] G. González de la Cruz, G. Contreras-Puente, F.L. Castillo-Alvarado, C. Mejfa-García, and A. Compaan, Solid State Commun. **82**, 927 (1992).

[29] A. Othonos, Ph.D. thesis, University of Toronto, 1990 (unpublished).

[30] R.K. Ray, R.L. Aggarwal, and B. Lax, in *Proceedings of the Second International Conference on Light Scattering in Solids*, edited by M. Balkanski (Flammarion Science, Paris, 1971), p. 288.

[31] M. Lax, Appl. Phys. Lett. **33** 787 (1978).

[32] J.F. Young and P.J. Kelly, Phys. Rev. B **47**, 6316 (1993).

[33] N.G. Nilsson, Appl. Phys. Lett. **33**, 653 (1978).

[34] E.O. Kane, J. Phys. Chem. Solids **1**, 82 (1956).

[35] E.M. Conwell and M.O. Vassel, Phys. Rev. **166**, 797 (1968).